International Journal of GEOMATE, Aug., 2024 Vol.27, Issue 120, pp.77-84
ISSN: 2186-2982 (P), 2186-2990 (O), Japan, DOI: https://doi.org/10.21660/2024.120.4541
Geotechnique, Construction Materials and Environment

TRANSIENT ANALYSIS OF FUNCTIONALLY GRADED NANOPLATES WITH POROSITIES TAKING INTO ACCOUNT SURFACE STRESS

Thanh-Binh Chu[1], *Xuan-Hung Dang[1], Van-Long Nguyen[1], Xuan-Trung Dang[1] and Minh-Tu Tran[1]

[1]Building and Industrial Construction Faculty, Hanoi University of Civil Engineering, Vietnam

*Corresponding Author, Received: 01 May 2024, Revised: 29 May 2024, Accepted: 30 May 2024

ABSTRACT: This paper presents a novel study on the transient response of simply supported rectangular functionally graded nanoplates with porosities. Nonlocal elasticity theory is employed in the analysis, incorporating the effect of surface energy. The motion equations of the nanoplates are derived from Hamilton's principle within the framework of Reddy's higher-order shear deformation theory. The closed-form solutions are obtained for transient analysis under diverse impulsive loading scenarios using Navier's technique. A very good agreement between the results of the present model and those available in the literature is found. This study reveals that the transient response of the nanoplate is significantly influenced by various factors, including nonlocal parameters, surface elastic constants, porosity distribution patterns, and elastic foundation stiffness. Notably, the surface energy effect has a greater impact on vibration amplitude compared to the nonlocal effect. The approach presented in this paper could serve as a valuable benchmark for the design, production, and operation of such nanoplates

Keywords: Nanoplate, Nonlocal elasticity theory, Surface elasticity theory, FGM with porosity, Transient analysis.

1. INTRODUCTION

Functionally graded materials (FGMs) are a class of advanced composite materials distinguished by their smoothly and continuously varying mechanical properties along specific directions. Typical FGMs are composed of ceramic and metallic constituents**.** The ceramic constituent offers high thermal resistance, while the metallic constituent provides ductility. These outstanding properties have led to the widespread application of FGMs in advanced technologies.

Micro/nanostructures made of FGM can be found in micro/nano electro-mechanical systems (MEMs or NEMs), sensors, actuators, gyroscopes, microphones, energy harvesting, and many other realms. Studies have shown that at the micro/nanoscale, the mechanical behavior of the structures differs significantly from that at the macro scale. In other words, the mechanical characteristics of micro/nanostructures depend on their extrinsic and intrinsic sizes. Classical elasticity theories cannot anticipate size effects due to the absence of inherent length scales, resulting in inaccuracies when applied to micro/nanoscale issues. Hence, alternative continuum theories beyond the classical ones, such as nonlocal elasticity theory, couple stress theory, and modified couple stress theory [1-3] as well as strain gradient theory and nonlocal strain gradient theory [4, 5] have been introduced.

During the production of FGMs, microvoids or porosity can emerge within the material. This phenomenon primarily arises from the differing solidification temperatures of the constituent materials used in FGMs, leading to the formation of these microvoids or porosities during the manufacturing process. The presence of these microvoids or porosities within the material reduces the mechanical strength of the plate, potentially leading to structural failure. Among size-dependent continuum theory for small-scale structures, Eringen's nonlocal elasticity theory is the most widely applied. A thorough understanding of the vibration response of nanostructures plays an important role in the design of MEM/NEM devices. Several outstanding studies regarding the vibration analysis of FGM nano-plates/shells with porosities (FGMPo) can be examined herein.

Based on first-order shear deformation theory (SDT), Vinh and Huy [6] investigated the effect of porosity and nonlocal parameters on the free vibration of simply-supported FGMPo nanoplates employing the nonlocal elasticity theory (NET) and Navier's technique. Mechab et al. [7] investigated the small-scale effect and porosity effect on free vibration of nano FGM plate resting on Pasternak elastic foundation based on two-variable refined plate theory incorporating the NET. Based on higher-order SDT and NET, Pham et al. [8] presented isogeometric analysis (IGA) and artificial neural network prediction to study the small-scale and porosity effects of FGMPo nanoplates. Merdaci et al. [9] proposed analytical solutions for the free vibration analysis of simply supported FGMPo nanoplates using a four-variable higher-order SDT. Tran and Le [10] presented isogeometric analysis to explore the

free vibration and buckling behaviour of FGMPo nanoplates utilizing the first-order SDT and NET. Based on NET, Wang and Teng [11] investigated the effect of porosity, nonlocal parameters, temperature, and boundary conditions on natural frequencies and critical buckling loads of FGMPo nanoplates under thermo-mechanical loading using differential transformation method and classical plate theory.

As a structure diminishes in size, the proportion of surface area to volume within the structure becomes more pronounced. Consequently, the material characteristics of the boundary layers surrounding the elastic medium diverge from those of the bulk materials. The high surface-to-bulk ratio of the nanostructures leads to exhibiting different behaviors compared to the conventional structures because of the considerable influence of the surface stress effect. In the surface theory of elasticity pioneered by Gurtin and Murdoch [12], the surface layer of a solid is conceptualized as a mathematically thin layer with distinct material properties compared to the underlying bulk material, effectively connected like a membrane. Utilizing this theory, the surface stress effect was examined in various FGM nanostructures.

For example, using the Generalized differential quadrature method, Ebrahim and Heidari [13] examined the effect of material, geometric, small-scale, and surface parameters on the nonlinear free vibrational characteristics of FGM rectangular nanoplate resting on Pasternak substrate according to third-order SDT. Norouzzadeh and Ansari [14] investigated size-dependent and surface stress effects on circular and rectangular FGM nanoplate by using IGA within the framework of first-order SDT in conjunction with nonlocal and surface stress elasticity theories. Employing a multiple-scale perturbation technique, Allahyari et al. [15] studied small-scale and surface stress effects on the nonlinear vibration response of FGM rectangular nanoplate under two types of simply supported boundary conditions. Based upon higher-order SDT quasi-3D plate theory and taking into account the surface stress type of size effect, Wang et al. [16] analyzed the nonlinear vibration response of variable thickness FGM nanoplates with different shapes using IGA.

The abovementioned review shows that there have been many studies on size-dependent effects and surface stress effects on the free vibrations of perfect FGM nanoplates. However, research on the influence of porosity on the vibrational characteristics of FGMPo nanoplates considering the surface energy effect has not been mentioned. Therefore, this paper aims to present an analytical approach to investigate both the nonlocal and surface energy effects on the transient response of perfect (FGM) and imperfect FGMPo nanoplate based on Reddy's third-order SDT. The numerical investigation is conducted to evaluate the effect of elastic foundation coefficient, porosity distribution patterns, surface stress, as well as nonlocal parameters on the transient response of FGMPo nanoplates.

2. RESEARCH SIGNIFICANCE

Understanding the influence of porosity on the mechanical behavior of FGMPo is critical for accurate structural performance analysis. While previous research has explored the free vibrations of FGM nanoplates, forced vibration analysis remains absent in the current literature. This study addresses this gap by presenting, for the first time, a dynamic response analysis of these nanoplates. The analysis utilizes a model based on nonlocal elasticity theory, incorporating the surface energy effect within the framework of Reddy's third-order SDT. Considering size-dependent and surface energy effects, the proposed model can be a valuable tool for analysts and designers to achieve more accurate predictions of the transient response in FGMPo nanoplates.

3. THEORETICAL FORMULATION

3.1. FGM nanoplate with porosities

An FGMPo nanoplate of length a, width b and thickness h is depicted in Fig. 1. The FGMPo nanoplate with a bottom layer is metal-rich (denoted by S^- at $z = -h/2$), and the top layer is ceramic-rich (denoted by S^+ at $z = h/2$) resting on Pasternak elastic foundation with Winkler stiffness k_w, and shear stiffness k_{si} ($i = x, y$).

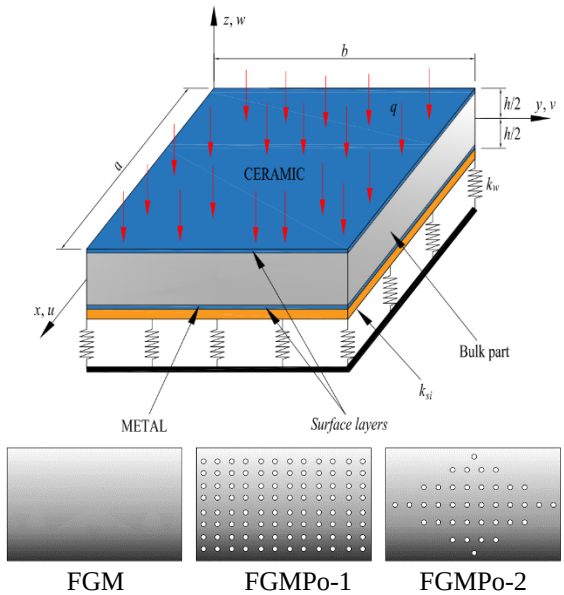

FGM FGMPo-1 FGMPo-2

Fig.1 FGM nanoplate with porosities resting on Pasternak elastic foundation

The effective material properties P (Young modulus E, mass density ρ, Poisson ratio v) of FGM

with and without porosities are determined by [17]

- Perfect FGM:

$$P(z)=P_{cm}\left(\frac{z}{h}+\frac{1}{2}\right)^{p}+P_{m} \quad (1)$$

- Imperfect Even FGM (FGMPo-1):

$$P(z)=P_{cm}\left(\frac{z}{h}+\frac{1}{2}\right)^{p}+P_{m}-\frac{e}{2}\left(P_{c}+P_{m}\right) \quad (2)$$

- Imperfect Uneven FGM (FGMPo-2):

$$P(z)=P_{cm}\left(\frac{z}{h}+\frac{1}{2}\right)^{p}+P_{m}-\frac{e}{2}\left(P_{c}+P_{m}\right)g(z) \quad (3)$$

where: $g(z)=1-\frac{2|z|}{h}; P_{cm}=P_{c}-P_{m}$; P_{c},P_{m} are the properties of the ceramic and metal, respectively; p is volume fraction index ($p \geq 0$); e is porosity coefficient ($0 \leq e \square 1$).

Two thin surface layers are considered in the upper and lower surfaces of FGMPo nanoplate with the surface parameters: $\mu^{s\pm},\lambda^{s\pm},\tau^{s\pm},\rho^{s\pm}$, and set:

$$\mu_t=\mu^{s+}+\mu^{s-};\ \mu_b=\mu^{s+}-\mu^{s-};\ \lambda_t=\lambda^{s+}+\lambda^{s-};$$
$$\lambda_b=\lambda^{s+}-\lambda^{s-};\ \tau_t=\tau^{s+}+\tau^{s-};\ \tau_b=\tau^{s+}-\tau^{s-};$$
$$\rho_t=\rho^{s+}+\rho^{s-};\ \rho_b=\rho^{s+}-\rho^{s-}.$$

3.2. Governing equations

Reddy's third-order SDT is a popular choice for plate analysis because it has the same number of displacement unknowns as first-order SDT but does not need to use a shear correction factor, and it also satisfies the condition of zero transverse shear stress at the top and bottom surfaces of plates. The displacements u,v,w of any point along (x, y, z) axes are expressed as [18]:

$$u=u_0(x,y,t)+z\theta_x(x,y,t)-\kappa z^3\left(\theta_x+\frac{\partial w_0}{\partial x}\right);$$
$$v=v_0(x,y,t)+z\theta_y(x,y,t)-\kappa z^3\left(\theta_y+\frac{\partial w_0}{\partial y}\right); \quad (4)$$
$$w=w_0(x,y,t)$$

where u_0,v_0,w_0 are displacements of any point in mid-plane along (x, y, z) axes; θ_x,θ_y are rotations of normal about y, x axes, and $\kappa=4/\left(3h^2\right)$.

The displacement-strain relations are expressed as

$$\begin{Bmatrix}\varepsilon_x\\ \varepsilon_y\\ \gamma_{xy}\end{Bmatrix}=\begin{Bmatrix}\varepsilon_x^0\\ \varepsilon_y^0\\ \gamma_{xy}^0\end{Bmatrix}+z\begin{Bmatrix}\kappa_x\\ \kappa_y\\ \kappa_{xy}\end{Bmatrix}-\kappa z^3\begin{Bmatrix}\kappa_x^*\\ \kappa_y^*\\ \kappa_{xy}^*\end{Bmatrix}; \quad (5)$$
$$\begin{Bmatrix}\gamma_{xz}\\ \gamma_{yz}\end{Bmatrix}=\left(1-3\kappa z^2\right)\begin{Bmatrix}\gamma_{xz}^0\\ \gamma_{yz}^0\end{Bmatrix}$$

where: $\varepsilon_x^0=\frac{\partial u_0}{\partial x};\varepsilon_y^0=\frac{\partial v_0}{\partial y};\gamma_{xy}^0=\frac{\partial u_0}{\partial y}+\frac{\partial v_0}{\partial x};$

$$\kappa_x=\frac{\partial\theta_x}{\partial x};\kappa_y=\frac{\partial\theta_y}{\partial y};\kappa_{xy}=\frac{\partial\theta_x}{\partial y}+\frac{\partial\theta_y}{\partial x};$$

$$\kappa_x^*=\frac{\partial\theta_x}{\partial x}+\frac{\partial^2 w_0}{\partial x^2};\kappa_y^*=\frac{\partial\theta_y}{\partial y}+\frac{\partial^2 w_0}{\partial y^2};$$

$$\kappa_{xy}^*=\frac{\partial\theta_x}{\partial y}+\frac{\partial\theta_y}{\partial x}+2\frac{\partial^2 w_0}{\partial x\partial y};$$

$$\gamma_{xz}^0=\frac{\partial w_0}{\partial x}+\theta_x;\gamma_{yz}^0=\frac{\partial w_0}{\partial y}+\theta_y.$$

Utilizing the nonlocal elasticity [19] and Gurtin-Murdoch surface theories [12, 20], the constitutive equations of the nanoplate for the bulk part can be expressed as follows

$$\Re\begin{Bmatrix}t_x\\ t_y\\ t_{xy}\end{Bmatrix}=\begin{bmatrix}Q_a & Q_b & 0\\ Q_b & Q_a & 0\\ 0 & 0 & Q_c\end{bmatrix}\begin{Bmatrix}\varepsilon_x\\ \varepsilon_y\\ \gamma_{xy}\end{Bmatrix}+\hat{\sigma}_z\begin{Bmatrix}Q_0\\ Q_0\\ 0\end{Bmatrix};$$
$$\Re\begin{Bmatrix}t_{xz}\\ t_{yz}\end{Bmatrix}=\begin{bmatrix}Q_c & 0\\ 0 & Q_c\end{bmatrix}\begin{Bmatrix}\gamma_{xz}\\ \gamma_{yz}\end{Bmatrix} \quad (6)$$

where: $\Re=1-\mu^2\nabla^2$; μ is the nonlocal coefficient.

$$\hat{\sigma}_z=\sigma_z^0+z\sigma_z^*;\ Q_a=\frac{E(z)}{1-\nu^2(z)};\ Q_b=\frac{\nu(z)E(z)}{1-\nu^2(z)};$$

$$Q_c=\frac{E(z)}{2\left[1+\nu(z)\right]};\ Q_0=\frac{\nu(z)}{1-\nu(z)};$$

$$\sigma_z^0=\frac{\tau_b}{2}\nabla^2 w_0-\frac{\rho_b}{2}\ddot{w}_0;\sigma_z^*=\frac{\tau_t}{h}\nabla^2 w_0-\frac{\rho_t}{h}\ddot{w}_0;$$

Similarly, the constitutive equations for the two surface layers can be expressed as

$$\Re t_x^{s\pm}=\tau^{s\pm}+\left(\lambda^{s\pm}+2\mu^{s\pm}\right)\varepsilon_x^{s\pm}+\left(\lambda^{s\pm}+\tau^{s\pm}\right)\varepsilon_y^{s\pm}$$
$$\Re t_y^{s\pm}=\tau^{s\pm}+\left(\lambda^{s\pm}+\tau^{s\pm}\right)\varepsilon_x^{s\pm}+\left(\lambda^{s\pm}+2\mu^{s\pm}\right)\varepsilon_y^{s\pm}$$
$$\Re t_{xy}^{s\pm}=\left(\mu^{s\pm}-\tau^{s\pm}\right)\gamma_{xy}^{s\pm}+\tau^{s\pm}\frac{\partial u^{s\pm}}{\partial y}; \quad (7)$$
$$\Re t_{yx}^{s\pm}=\left(\mu^{s\pm}-\tau^{s\pm}\right)\gamma_{xy}^{s\pm}+\tau^{s\pm}\frac{\partial v^{s\pm}}{\partial x};$$
$$\Re t_{xz}^{s\pm}=\tau^{s\pm}\frac{\partial w_0}{\partial x};\ \Re t_{yz}^{s\pm}=\tau^{s\pm}\frac{\partial w_0}{\partial y}$$

The equations of motion of FGMPo nanoplate are derived from Hamilton's principle [21]:

$$0=\int_0^T\left(\delta U_P+\delta U_F-\delta K\right)dt \quad (8)$$

The variation of the strain energy of the FGMPo nanoplate can be calculated as:

$$\delta U_P=\int_V t_{ij}\delta\varepsilon_{ij}dV+\int_{S^+}t_{ij}^{s+}\delta\varepsilon_{ij}dS+\int_{S^-}t_{ij}^{s-}\delta\varepsilon_{ij}dS \quad (9)$$

The variation of the strain energy of the foundation is given as:

$$\delta U_F = \int_A \left(k_w w_0 - k_{sx} \frac{\partial^2 w_0}{\partial x^2} - k_{sy} \frac{\partial^2 w_0}{\partial y^2} \right) \delta w_0 dA \quad (10)$$

The variation of kinetic energy:

$$\delta K = \int_V \rho \dot{u}_i \delta \dot{u}_i dV + \int_{S^+} \rho^{s+} \dot{u}_i \delta \dot{u}_i dS + \int_{S^-} \rho^{s-} \dot{u}_i \delta \dot{u}_i dS \quad (11)$$

By substituting Eqs. (9)-(11) into Eq. (8), the equations of motion are obtained:

$$\frac{\partial N_x}{\partial x} + \frac{\partial N_{xy}}{\partial y} = m_0 \ddot{u}_0 + m_{1a} \ddot{\theta}_x - m_{1b} \frac{\partial \ddot{w}_0}{\partial x};$$

$$\frac{\partial N_{xy}}{\partial x} + \frac{\partial N_y}{\partial y} = m_0 \ddot{v}_0 + m_{1a} \ddot{\theta}_y - m_{1b} \frac{\partial \ddot{w}_0}{\partial y};$$

$$\kappa \left(\frac{\partial^2 M_x^*}{\partial x^2} + 2 \frac{\partial M_{xy}^*}{\partial x \partial y} + \frac{\partial^2 M_y^*}{\partial y^2} \right) + \frac{\partial R_x}{\partial x} + \frac{\partial R_y}{\partial y} + \frac{\partial R_x^s}{\partial x} + \frac{\partial R_y^s}{\partial y} + q - k_w w_0 + k_{sx} \frac{\partial^2 w_0}{\partial x^2} + k_{sy} \frac{\partial^2 w_0}{\partial y^2} = m_{1b} \left(\frac{\partial \ddot{u}_0}{\partial x} + \frac{\partial \ddot{v}_0}{\partial y} \right) + m_0 \ddot{w}_0 - m_{2c} \nabla \ddot{w}_0 + m_{2a} \left(\frac{\partial \ddot{\theta}_x}{\partial x} + \frac{\partial \ddot{\theta}_y}{\partial y} \right); \quad (12)$$

$$\frac{\partial P_x}{\partial x} + \frac{\partial P_{xy}}{\partial y} - R_x = m_{1a} \ddot{u}_0 - m_{2a} \frac{\partial \ddot{w}_0}{\partial x} + m_{2b} \ddot{\theta}_x;$$

$$\frac{\partial P_y}{\partial y} + \frac{\partial P_{xy}}{\partial x} - R_y = m_{1a} \ddot{v}_0 - m_{2a} \frac{\partial \ddot{w}_0}{\partial y} + m_{2b} \ddot{\theta}_y$$

where : $P_i = M_i - \kappa M_i^*, i = x, y, xy.$

The stress resultants are defined as:

$$\begin{bmatrix} N_x & M_x & M_x^* \\ N_y & M_y & M_y^* \\ N_{xy} & M_{xy} & M_{xy}^* \end{bmatrix} = \int_{-h/2}^{h/2} \begin{Bmatrix} t_x \\ t_y \\ t_{xy} \end{Bmatrix} \begin{bmatrix} 1 & z & z^2 \end{bmatrix} dz + \begin{Bmatrix} t_x^{s+} + t_x^{s-} \\ t_y^{s+} + t_y^{s-} \\ t_{xy}^{s+} + t_{yx}^{s+} + t_{xy}^{s-} + t_{yx}^{s-} \end{Bmatrix} \begin{bmatrix} 1 & \frac{h}{2} & \frac{h^3}{8} \end{bmatrix}; \quad (13)$$

$$\begin{Bmatrix} R_x \\ R_y \end{Bmatrix} = \int_{-h/2}^{h/2} \begin{Bmatrix} t_{xz} \\ t_{yz} \end{Bmatrix} \left(1 - 3\kappa z^2 \right) dz;$$

$$\begin{Bmatrix} R_x^s \\ R_y^s \end{Bmatrix} = \begin{Bmatrix} t_{xz}^{s+} + t_{xz}^{s-} \\ t_{yz}^{s+} + t_{yz}^{s-} \end{Bmatrix}$$

The mass of inertia is defined as follows:

$$m_0 = I_0 + \rho_t; m_{1a} = J_1 + \frac{h}{3} \rho_b;$$

$$m_{1b} = \kappa I_3 + \frac{h}{6} \rho_b; m_{2a} = \kappa J_4 + \frac{h^2}{18} \rho_t; \quad (14)$$

$$m_{2b} = K_2 + \frac{h^2}{9} \rho_t; m_{2c} = \kappa^2 I_6 + \frac{h^2}{36} \rho_t;$$

$$I_0 = \int_{-h/2}^{h/2} \rho z^i dz; i = 0 \div 4, 6; J_1 = I_1 - \kappa I_3;$$

$$J_4 = I_4 - \kappa I_6; K_2 = I_2 - 2\kappa I_4 + \kappa^2 I_6$$

3.3. Navier's solution

Let's consider the simply supported (SS) rectangular FGMPo nanoplates. The associated boundary conditions (BCs) are as follows:

At $x = 0$ and $x = a$:

$$v_0 = w_0 = \theta_y = N_x = M_x^* = \frac{\partial w_0}{\partial y} = M_x = 0$$

At $y = 0$ and $y = b$: (15)

$$u_0 = w_0 = \theta_x = N_y = M_y^* = \frac{\partial w_0}{\partial x} = M_y = 0$$

The displacement unknowns are chosen to satisfy the boundary condition (15) in the following forms:

$$u_0 = \sum_{m=1}^{\infty} \sum_{n=1}^{\infty} u_{0mn}(t) \cos(\lambda x) \sin(\beta y);$$

$$v_0 = \sum_{m=1}^{\infty} \sum_{n=1}^{\infty} v_{0mn}(t) \sin(\lambda x) \cos(\beta y);$$

$$w_0 = \sum_{m=1}^{\infty} \sum_{n=1}^{\infty} w_{0mn}(t) \sin(\lambda x) \sin(\beta y); \quad (16)$$

$$\theta_x = \sum_{m=1}^{\infty} \sum_{n=1}^{\infty} \theta_{xmn}(t) \cos(\lambda x) \sin(\beta y);$$

$$\theta_y = \sum_{m=1}^{\infty} \sum_{n=1}^{\infty} \theta_{ymn}(t) \sin(\lambda x) \cos(\beta y)$$

in which: $\lambda = \frac{m\pi}{a}, \beta = \frac{n\pi}{b}$; $m, n = 1, 2, 3, ...$; u_{0mn}, $v_{0mn}, w_{0mn}, \theta_{xmn}, \theta_{ymn}$ are unknown coefficients.

The transverse applied loads $q(x, y, t)$ are also expanded in double trigonometric Fourier series as follows:

$$q(x, y, t) = \sum_{m=1}^{\infty} \sum_{n=1}^{\infty} q_{mn}(t) \sin(\lambda x) \sin(\beta y) \quad (17)$$

in which:

$$q_{mn}(t) = \frac{4}{ab} \int_0^a \int_0^b q(x, y, t) \sin(\lambda x) \sin(\beta y) dx dy \quad (18)$$

Applying the operator $\Re$ to Eqs. (12), and using the relations (5)-(7), the equations of motion in terms of displacements are obtained. Then, substituting Eqs. (16) and (17) into the equations of motion in terms of displacements, the system of algebraic equations is obtained in the following matrix form:

$$\boldsymbol{K}\boldsymbol{Q}(t) + \boldsymbol{M}\ddot{\boldsymbol{Q}}(t) = \boldsymbol{F}(t) \quad (20)$$

where $\boldsymbol{K}$ and $\boldsymbol{M}$ are the stiffness and mass matrix of the FGMPo nanoplate; $\boldsymbol{F}(t)$ is the external load

vector; $\boldsymbol{Q}(t)$ is a vector of unknown coefficients.

The system of equations (20) is used to analyze the dynamic response of FGMPo plates according to Reddy's third-order shear deformation theory. The Runge-Kutta method with initial conditions $\boldsymbol{Q}(0)=\boldsymbol{0}$, $\dot{\boldsymbol{Q}}(0)=\boldsymbol{0}$ will be applied to obtain the transient response of the plates.

4. NUMERICAL RESULTS

4.1. Validation Example

The linear dynamic analysis of an isotropic square plate subjected to a uniformly distributed step load (load intensity q = 48.82 Pa, suddenly acted at the time t_1 = 0 and lasts t_2 = 0.2 s) with SS-BCs is conducted. The time history curves of the central deflection of a square isotropic plate obtained from the present approach and the quadrature element method given by Shen et al. [22] are in good agreement, as illustrated in Figure 2. Also, note that the size effects have been ignored in this example.

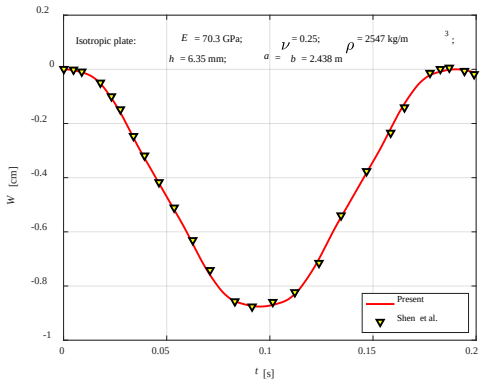

Fig. 2 The time histories of central deflection of the isotropic plates under step uniformly distributed load.

4.2. Parametric study

In this section, the rectangular FGMPo nanoplate resting on the Pasternak elastic foundation is considered. FGMPo is composed of ceramic (Si) and metal (Al) with material properties and surface parameters given in References [23].

For convenience, the following nondimensional parameters are used [24]:

$$\overline{w}(t)=\frac{10E_c h^3}{q_0 a^4}w_0\left(\frac{a}{2},\frac{b}{2},t\right);\ t^*=\frac{t}{t_s};$$
$$K_0=\frac{k_w a^4}{E_0 h^3};J_0=\frac{k_{sx}a^2}{\nu_m E_0 h^3}=\frac{k_{sy}b^2}{\nu_m E_0 h^3};\quad (18)$$
$$t_s=0.1\text{ns};\ E_0=1\,\text{GPa}$$

The dynamic response of FGMPo nanoplate under different types of pulse loads including:

- Step loading [25]:

$$q_0(t)=\begin{cases}p_0; & \left(0\le t\le rt_p\right)\\ 0; & \left(t<0,t>rt_p\right)\end{cases}\quad (19)$$

in which: p_0 is the initial value of the load, r is the shock pulse length factor, and t_p is the loading time.

- Sinusoidal loading [25]:

$$q_0(t)=\begin{cases}p_0\sin\dfrac{\pi t}{rt_p}; & \left(0\le t\le rt_p\right)\\ 0; & \left(t<0,t>rt_p\right)\end{cases}\quad (20)$$

- Triangular loading [25]:

$$q_0(t)=\begin{cases}p_0\left(1-t/t_p\right); & \left(0\le t\le rt_p\right)\\ 0; & \left(t<0,t>rt_p\right)\end{cases}\quad (21)$$

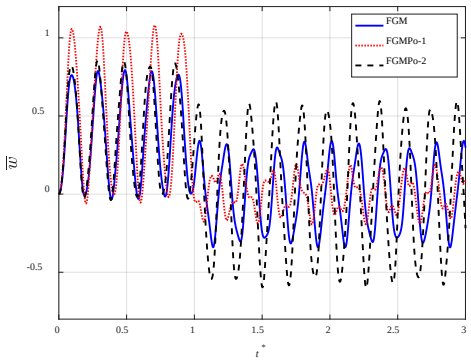

(a) Step load

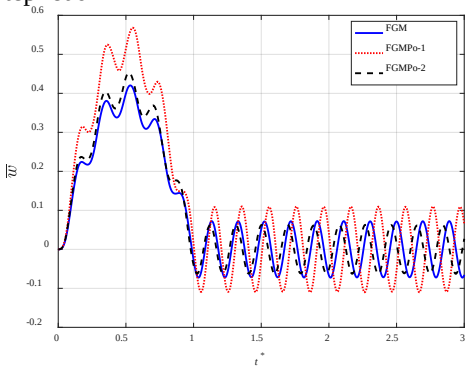

(b) Sinusoidal load

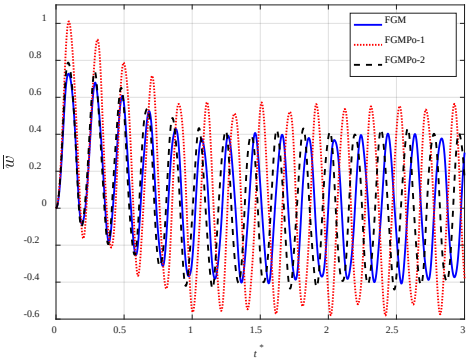

(c) Triangular load

Fig. 3 Effect of porosity distribution patterns on the dynamic response of FGM nanoplate.

Consider FGMPo nanoplates (a = 10 nm, a/h = 10, b/a = 1) subjected to a uniform transverse load $q(x,y,t) = q_0(t)$. The input data are p = 2, e = 0.3, μ = 1 nm, t_p = 0.1 ns, and r = 1.

Figures 3 (a), (b) and (c) show the effect of porosity distribution patterns on the dynamic response of FGM nanoplate under different types of shock pulse loadings. Both nonlocal and surface effects are considered in the analysis.

Under step loading, the presence of porosity reduces the stiffness of the nanoplate, leading to increased deflection compared to a perfect FGM nanoplate. Interestingly, during load application, the uneven porosity distribution (FGMPo-2) results in smaller deflection or vibration amplitude compared to the even distribution (FGMPo-1). However, after the load is removed, the FGMPo-1 pattern exhibits a larger decrease in deflection, suggesting a better ability to absorb the step load due to its even porosity distribution. This is because even porosity distribution spreads porosities across the whole cross-section, while the uneven distribution concentrates them away from the corners.

For sinusoidal and triangular loads, it is evident that the perfect FGM nanoplate possesses the smallest deflection and FGMPo-1 nanoplate yields a larger deflection than FGMPo-2.

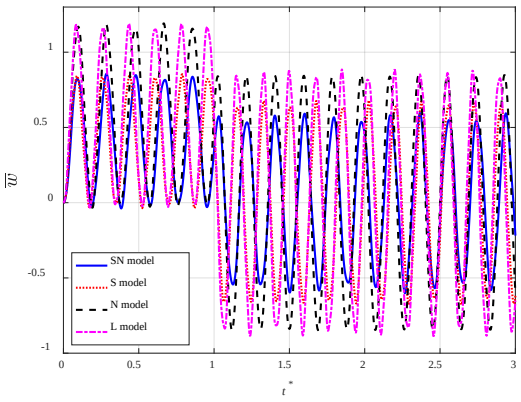

(a) Step load

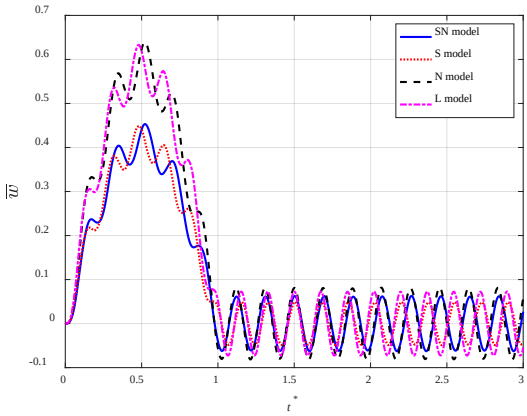

(b) Sinusoidal load

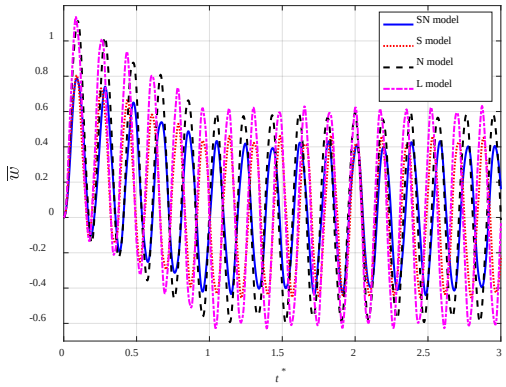

(c) Triangular load

Fig. 4 Dynamic response of FGMPo-2 nanoplate under different types of shock pulse loadings using various nonlocal models

Due to have superior bending stiffness, the FGMPo-2 pattern is chosen as the primary focus for investigating the influence of the remaining parameters on the transient response of nanoplates.

The effect of various size-dependent theories on the dynamic response of FGMPo-2 nanoplate can be observed in Figure 4 (a), (b), and (c). The result for the classical elasticity model is obtained when $\mu = 0$ and $\mu^{s\pm} = \lambda^{s\pm} = \tau^{s\pm} = \rho^{s\pm} = 0$.

For all three types of pulse loading, the surface effects significantly reduce deflection, resulting in the solid blue curve (both nonlocal and surface effect - SN model) and red dashed line (only surface effect - S model) having smaller amplitudes than the remaining two curves (only nonlocal effect - N model and classical theory - L model). The nonlocal effect slightly affects the vibration amplitudes of nanoplates.

Figures 5 (a), (b) and (c) illustrate the effect of the shock pulse length factor (r), which represents the loading time. Different types of shock pulse loadings and the SN model are utilized for investigation.

For step load, as r increases, leading to an increase in loading time, the maximum dynamic deflection of the nanoplate shows very little change. For sinusoidal loading, as r increases, the maximum pressure of the load remains unchanged, but the loading duration time is longer. Consequently, the maximum dynamic deflection of the nanoplate is reduced. For nanoplates subjected to triangular loads, r increases, the loading duration time becomes longer, and the maximum dynamic deflection of the plate also increases.

Figure 6 illustrates the effect of elastic foundation stiffnesses on the dynamic response of FGMPo-2 nanoplate under triangular loadings. It can be seen that increasing the elastic foundation coefficient (higher values of K_0 and J_0) leads to a decrease in plate deflection as expected.

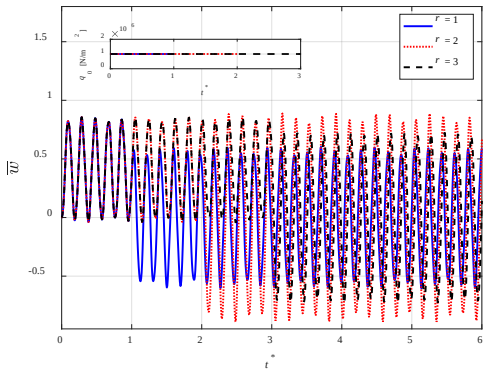

(a) Step load

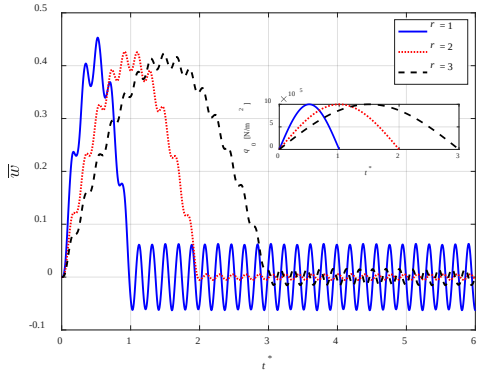

(b) Sinusoidal load

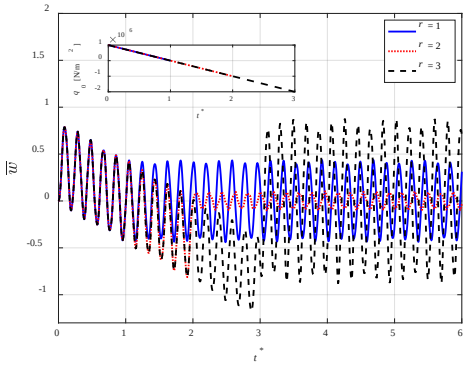

(c) Triangular load

Fig. 5 Effect of pulse length factor *r* on the dynamic response of FGMPo-2 nanoplate

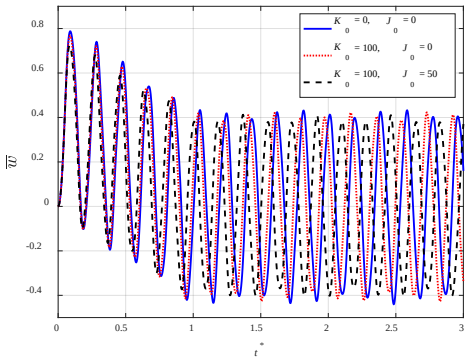

Fig. 3 Effect of elastic foundation on the dynamic response of FGMPo-2 nanoplate under triangular loads

5. CONCLUSIONS

The paper develops an analytical solution to analyze the transient response of the FGMPo nanoplate resting on a Pasternak elastic foundation, taking into account both the nonlocal size-dependent effect and surface energy effects simultaneously. Several numerical examples are presented to indicate the effect of porosity distribution patterns, surface stress, nonlocal parameters, as well as elastic foundation coefficients on the transient response of FGMPo nanoplates. The main findings can be summarized as follows:

- The surface effects (S model) significantly affect vibration amplitudes. In contrast, the nonlocal effect (N model) slightly affects vibration amplitudes.
- FGM nanoplates with uneven porosity distribution (FGMPo-2) exhibit higher stiffness compared to those with even porosity distribution. This translates to smaller deflection under pulse load for FGMPo-2 nanoplates compared to FGMPo-1 nanoplates.
- As the elastic foundation coefficients (K_0 and J_0) increase, the dynamic deflection decreases.

Despite its limitation to simply supported boundary conditions, Navier's solution remains a valuable tool for designing and fabricating MEM/NEM devices. This is because it effectively predicts the transient response of nanoplates. Furthermore, Navier's solution can serve as a basis for solving more complex problems, such as analyzing the thermal effects of FGMPo nanoplates under various boundary conditions.

6. ACKNOWLEDGMENTS

This research is funded by the Vietnam Ministry of Education and Training, project under grant number: B2022-XDA-04.

7. REFERENCES

[1] Yang, F. A. C. M., Chong, A. C. M., Lam, D. C. C., & Tong, P., Couple stress based strain gradient theory for elasticity. International journal of solids and structures, 2002. 39(10): p. 2731-2743.

[2] Park, S. and X. Gao, Bernoulli–Euler beam model based on a modified couple stress theory. Journal of Micromechanics and Microengineering, 2006. 16(11): p. 2355.

[3] Ma, H., X.-L. Gao, and J. Reddy, A microstructure-dependent Timoshenko beam model based on a modified couple stress theory. Journal of the Mechanics and Physics of Solids, 2008. 56(12): p. 3379-3391.

[4] Fleck, N. A., Muller, G. M., Ashby, M. F., & Hutchinson, J. W., Strain gradient plasticity:

theory and experiment. Acta Metallurgica et materialia, 1994. 42(2): p. 475-487.
[5] Barati, M.R., A general nonlocal stress-strain gradient theory for forced vibration analysis of heterogeneous porous nanoplates. European Journal of Mechanics-A/Solids, 2018. 67: p. 215-230.
[6] Vinh, P.V. and L.Q. Huy, Influence of variable nonlocal parameter and porosity on the free vibration behavior of functionally graded nanoplates. Shock and Vibration, 2021. 2021: p. 1-17.
[7] Mechab, I., Mechab, B., Benaissa, S., Serier, B., & Bouiadjra, B. B., Free vibration analysis of FGM nanoplate with porosities resting on Winkler Pasternak elastic foundations based on two-variable refined plate theories. Journal of the Brazilian Society of Mechanical Sciences and Engineering, 2016. 38: p. 2193-2211.
[8] Pham, Q.-H., T.T. Tran, and P.-C. Nguyen, Nonlocal free vibration of functionally graded porous nanoplates using higher-order isogeometric analysis and ANN prediction. Alexandria Engineering Journal, 2023. 66: p. 651-667.
[9] Slimane, M., Mostefa, A. H., Boutaleb, S., & Hellal, H., Free Vibration Analysis of Functionally Graded FG Nano-Plates with Porosities. Journal of Nano Research, 2020. 64: p. 61-74.
[10] Tran, M.T. and T.C. Le, A nonlocal IGA numerical solution for free vibration and buckling analysis of porous sigmoid functionally graded (P-SFGM) nanoplate. International Journal of Structural Stability and Dynamics, 2022. 22(16): p. 2250193.
[11] Wang, W. and Z. Teng, Analysis of vibration and critical buckling load of porous functionally graded material rectangular nanoplates under thermo-mechanical loading. ZAMM-Journal of Applied Mathematics and Mechanics/Zeitschrift für Angewandte Mathematik und Mechanik, 2024. 104(1): p. e202200073.
[12] Gurtin, M.E. and A. Ian Murdoch, A continuum theory of elastic material surfaces. Archive for rational mechanics and analysis, 1975. 57: p. 291-323.
[13] Ebrahimi, F. and E. Heidari, Surface effects on nonlinear vibration of embedded functionally graded nanoplates via higher order shear eformation plate theory. Mechanics of Advanced Materials and Structures, 2019. 26(8): p. 671-699.
[14] Norouzzadeh, A. and R. Ansari, Isogeometric vibration analysis of functionally graded nanoplates with the consideration of nonlocal and surface effects. Thin-Walled Structures, 2018. 127: p. 354-372.
[15] Allahyari, E., M. Asgari, and A.A. Jafari, Nonlinear size-dependent vibration behavior of graphene nanoplate considering surfaces effects using a multiple-scale technique. Mechanics of Advanced Materials and Structures, 2020. 27(9): p. 697-706.
[16] Wang, P., Yuan, P., Sahmani, S., & Safaei, B., Surface stress size dependency in nonlinear free oscillations of FGM quasi-3D nanoplates having arbitrary shapes with variable thickness using IGA. Thin-Walled Structures, 2021. 166: p. 108101.
[17] Wattanasakulpong, N. and V. Ungbhakorn, Linear and nonlinear vibration analysis of elastically restrained ends FGM beams with porosities. Aerospace Science and Technology, 2014. 32(1): p. 111-120.
[18] Reddy, J.N., Theory and analysis of elastic plates and shells. 2006: CRC Press.
[19] Eringen, A.C. and D. Edelen, On nonlocal elasticity. International journal of engineering science, 1972. 10(3): p. 233-248.
[20] Gurtin, M.E. and A.I. Murdoch, Surface stress in solids. International Journal of Solids and Structures, 1978. 14(6): p. 431-440.
[21] Reddy, J.N., Energy principles and variational methods in applied mechanics. 2017: John Wiley & Sons.
[22] Shen, Z., J. Xia, and P. Cheng, Geometrically nonlinear dynamic analysis of FG-CNTRC plates subjected to blast loads using the weak form quadrature element method. Composite Structures, 2019. 209: p. 775-788.
[23] Miller, R.E. and V.B. Shenoy, Size-dependent elastic properties of nanosized structural elements. Nanotechnology, 2000. 11(3): p. 139.
[24] Zenkour, A.M., The refined sinusoidal theory for FGM plates on elastic foundations. International journal of mechanical sciences, 2009. 51(11-12): p. 869-880.
[25] Li, Z. N., Hao, Y. X., Zhang, W., & Zhang, J. H., Nonlinear transient response of functionally graded material sandwich doubly curved shallow shell using new displacement field. Acta Mechanica Solida Sinica, 2018. 31(1): p. 108-126.